

HPSTAR
068_2014

OPEN

SUBJECT AREAS:

PHASE TRANSITIONS
AND CRITICAL
PHENOMENASTRUCTURE OF SOLIDS AND
LIQUIDSReceived
23 September 2014Accepted
4 November 2014Published
24 November 2014Correspondence and
requests for materials
should be addressed to
L.W. (wanglin@hpstar.
ac.cn; lwang@
carnegiescience)

Conventional empirical law reverses in the phase transitions of 122-type iron-based superconductors

Zhenhai Yu¹, Lin Wang^{1,2,3}, Luhong Wang⁴, Haozhe Liu^{1,4}, Jinggeng Zhao⁴, Chunyu Li¹, Stanislav Sinogeikin⁵, Wei Wu⁶, Jianlin Luo^{6,7}, Nanlin Wang^{7,8}, Ke Yang⁹, Yusheng Zhao¹⁰ & Ho-kwang Mao^{1,5,11}

¹Center for High Pressure Science and Technology Advanced Research, Shanghai, 201203, China, ²State Key Laboratory of Superhard Materials, Jilin University, Changchun 130012, China, ³High Pressure Synergetic Consortium, Geophysical Laboratory, Carnegie Institution of Washington, Argonne, Illinois 60439, United States of America, ⁴Harbin Institute of Technology, Harbin 150080, China, ⁵High Pressure Collaborative Access Team, Geophysical Laboratory, Carnegie Institution of Washington, Argonne, Illinois 60439, United States of America, ⁶Beijing National Lab for Condensed Matter Physics, Institute of Physics, Chinese Academy of Sciences, Beijing 100190, China, ⁷Collaborative Innovation Center of Quantum Matter, Beijing, China, ⁸International Center for Quantum Materials, School of Physics, Peking University, Beijing 100871, China, ⁹Shanghai Institute of Applied Physics, Chinese Academy of Sciences, Shanghai 201203, China, ¹⁰High Pressure Science and Engineering Center, University of Nevada, Las Vegas, Nevada 89154, United States of America, ¹¹Geophysical Laboratory, Carnegie Institution of Washington, Washington DC 20015, United States of America.

Phase transition of solid-state materials is a fundamental research topic in condensed matter physics, materials science and geophysics. It has been well accepted and widely proven that isostructural compounds containing different cations undergo same pressure-induced phase transitions but at progressively lower pressures as the cation radii increases. However, we discovered that this conventional law reverses in the structural transitions in 122-type iron-based superconductors. In this report, a combined low temperature and high pressure X-ray diffraction (XRD) measurement has identified the phase transition curves among the tetragonal (T), orthorhombic (O) and the collapsed-tetragonal (cT) phases in the structural phase diagram of the iron-based superconductor AFe_2As_2 ($A = Ca, Sr, Eu, \text{ and } Ba$). The cation radii dependence of the phase transition pressure ($T \rightarrow cT$) shows an opposite trend in which the compounds with larger ambient radii cations have a higher transition pressure.

Phase transition of condensed matters is one of the most fundamental research topics in geoscience, material, physics and chemistry. External pressure is an important parameter in tuning the crystallographic structures of materials. There are some common characteristics for solids under pressure. Generally speaking, applying pressure decreases the volume and overall interatomic distances of the materials. One generally accepted rule is that isostructural compounds follow the similar phase transition sequence upon compression, such as the NaCl-type (B1) \rightarrow CsCl-type (B2) structural phase transition in alkaline earth metal oxides (CaO, SrO and BaO)^{1–4}. Another common rule states that the isostructural compounds containing different cations will undergo phase transitions at progressively lower pressures as the cation radii increases. For example, the pressure of phase transition ($Fm-3m \rightarrow Pnma$) in alkaline earth metal fluorides (CaF_2, SrF_2 and BaF_2) is $\sim 9, \sim 5$ and ~ 3 GPa^{5–7}, respectively. Here, we found that the pressure-induced structural phase transition in AFe_2As_2 ($A = Ca, Eu, Sr$ and Ba) did not follow this conventional rule.

Iron-based superconductors have attracted much attention because they not only exhibit high superconductivity transition temperatures like copper-based high temperature superconductors, but also because they are novel-type systems to study the interplay between magnetism and superconductivity^{8–12}. The $ThCr_2Si_2$ -type ternary AFe_2As_2 is known as the “122” system and has spurred interest because the iron is magnetic at low temperatures. Here, A is a divalent alkaline earth or rare earth metal, such as $Ca^{13}, Sr^{14}, Ba^{15}$ and Eu^{16} . The interesting crystallography of the AB_2X_2 -type (B is a transition metal or main group element and X comes from the groups 15, 14, occasionally 13.) compounds were highlighted in 1985 by R. Hoffmann and C. Zheng¹⁷. They pointed out that a segregation in this type of material occurs due to the presence or absence of interlayer X-X bonding. This results in either a “collapsed” or “uncollapsed” tetragonal structure, respectively.

$EuFe_2As_2$ is one of the $ThCr_2Si_2$ -type ternary superconductors that was synthesized three decades ago¹⁸. There has been little research on this topic until the discovery of iron-based superconductors. The $EuFe_2As_2$ is a poor



metal with room-temperature resistivity of $4 \times 10^{-4} \Omega \text{ cm}$ which is more than 2 orders of magnitude higher than that of normal metals such as iron. The EuFe_2As_2 is paramagnet at room temperature. Similar to BaFe_2As_2 and SrFe_2As_2 , Mössbauer and magnetic susceptibility studies revealed that EuFe_2As_2 undergoes two magnetic phase transitions at 200 and 20 K^{19–21}. The former is due to the antiferromagnetic transition in the iron sub-lattice. The latter arises from the antiferromagnetic ordering of the Eu^{2+} magnetic moments. The temperature dependent X-ray diffraction (XRD) of EuFe_2As_2 has been previously investigated and revealed a structural phase transition from the ambient condition tetragonal ThCr_2Si_2 -type phase to a low temperature orthorhombic β - SrRh_2As_2 -type structure at 190 K²².

Previous studies have shown that the applied pressure plays an important role in tailoring the superconductivity transition temperature on the recently discovered iron-based superconductors^{23–25}. For example, a second superconducting phase suddenly reemerges above 11.5 GPa in iron chalcogenides after the T_c drops from the first maximum of 32 K at 1 GPa²³. The T_c of EuFe_2As_2 shows a rapid increase between 4 and 10 GPa and reaches a maximum of 41 K near 10 GPa²⁵. The pressure-induced valence change of europium in EuFe_2As_2 was studied by L.L. Sun *et al.* using X-ray absorption measurements^{26,27}. Some *in situ* high pressure XRD experiments on EuFe_2As_2 have also been performed. For example, synchrotron XRD analysis shows that the EuFe_2As_2 undergoes a $T \rightarrow \text{cT}$ structural phase transition around 8 GPa. The structural phase transitions in EuFe_2As_2 at low temperatures and high pressures have also been reported²⁸. The $T \rightarrow \text{O}$ and $T \rightarrow \text{cT}$ structural phase transitions occurred at 4.3 GPa and 120 K, and at 11 GPa and 10 K, respectively.

The importance of the structural evolution of the AB_2X_2 -type compounds was highlighted by the relationship among magnetism, superconductivity and lattice instabilities in the iron arsenide family of superconductors. Although great efforts have been devoted to understand the temperature/pressure-induced structural phase transitions in AFe_2As_2 , the issue of first or second-order phase transition, phase transition temperature/pressure and the coexistence of phase have also been a matter of dispute. The crystal structure evolution in P - T domain of EuFe_2As_2 is still not fully known. To complement the above data, we have performed an XRD experiment with EuFe_2As_2 using a combined low temperature and high pressure XRD technique. Studies into the crystal structural evolution as a function of pressure were performed based on *in situ* high-pressure synchrotron XRD data and Rietveld refinement. This provides insights into the pressure effect on the crystal structures of the 122-type superconductor. Here we report details on the temperature- and pressure-induced structural phase transition in EuFe_2As_2 . Additionally, the transition pressure in AFe_2As_2 follows a trend in which the larger ambient cation radii have higher transition pressures. This does not follow the conventional empirical law.

Results

The EuFe_2As_2 high quality single crystals used here were grown using the Sn-flux method. The single crystals were ground in a mortar to obtain a fine powder sample for angle dispersive XRD experiments. Apart from the diffraction peak (123) in EuFe_2As_2 splitting into (400) and (040) around 190 K reported in the literature²², we also observed Bragg diffraction peaks (112) splitting into (202) and (022) by taking advantage of the high resolution synchrotron XRD diffraction technique at 11 BM-B at APS of ANL as shown in the supplementary materials (Fig. S1).

The variation in crystallographic structure for EuFe_2As_2 under high pressure and ambient temperature was investigated using a symmetric DAC. Figure 1 presents the selected AD-XRD patterns of EuFe_2As_2 under various pressures at 12 K. The (110) Bragg diffraction peak is on the right of (103) under low pressure

(< 14.3 GPa). This is shown by the red and blue arrows at the bottom of Figure 1. The (110) and (103) diffraction peaks merge into one peak (peak I) due to the limited resolution of the detector. As the pressure increases, the diffraction peaks (103) and (110) separate into two peaks (Peak II and III, on the top of Figure 1) due to the reverse movement. The relative intensity of the (103) Bragg diffraction peak is stronger than (110) across all pressures studied here. The Bragg diffraction peaks of (103) and (112) exhibit a movement to the higher diffraction angle as the pressure increases. On the contrary, the Bragg diffraction peaks (110) and (200) show a movement to the lower diffraction angle from 9.5 to 25.2 GPa. An important point to note is that the Bragg diffraction peaks (110) and (200) move to the lower diffraction angle (or higher d -spacing), which is clear evidence of the anomalous compression of the lattice parameter a in the tetragonal lattice.

The lattice parameters and atomic positions of EuFe_2As_2 under various pressures at 12 K were determined using Rietveld refinements (Figure 2a and 2b). The lattice parameters a and c of the T phase in EuFe_2As_2 show a normal decrease with pressure up to 9.5 GPa. At this juncture, a strong decrease is seen in the c lattice parameter to smaller values, after which a normal compression behavior is observed up to 31.5 GPa. However, as the pressure increases, anomalous compression effects were observed with the lattice parameter a expanding rapidly to around 25.2 GPa. Similar pressure-induced structural phase transition from a tetragonal to a collapsed tetragonal structure also occurs in EuFe_2P_2 under 9.8 GPa at ambient temperature²⁹.

Figure 2c exhibits the measured pressure dependence of volume for EuFe_2As_2 up to 31.5 GPa at 12 K. The P - V data was fitted to a Birch-Murnaghan equation of state³⁰. The fitted lattice volume is 184.0 \AA^3 for the T phase and 168.9 \AA^3 for the cT phase at 12 K, respectively. We found that this equation of state presents considerable decreases in compressibility between the tetragonal and the high-pressure collapsed tetragonal phase. This is seen in the variation of slope for the pressure-volume (P - V) curve separated by 12 GPa. This indicates that the cT phase has lower compressibility than that of the T phase. With B_0' fixed to be 4, we obtained ambient pressure isothermal bulk modulus of $B_0 = 58.1(2.3)$ and $160.0(3.0)$ GPa for the T and cT phase of the EuFe_2As_2 , respectively. We only did the

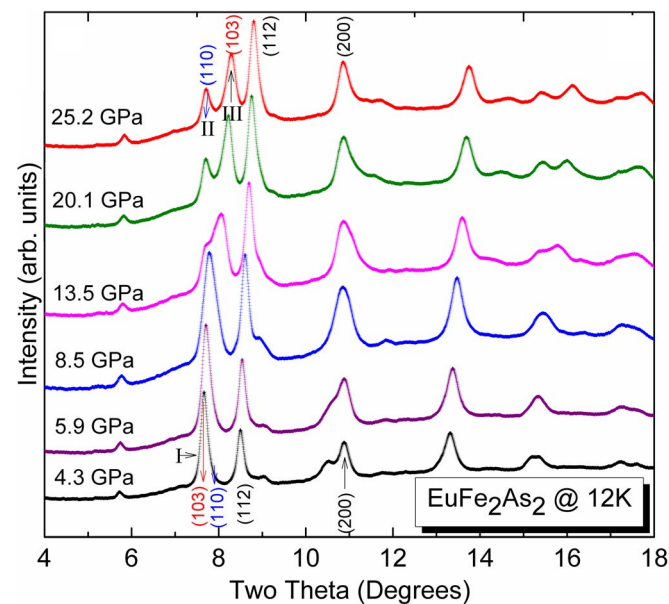


Figure 1 | Selected AD-XRD pattern of EuFe_2As_2 under various pressures at 12 K. A pressure-induced isostructural phase transition in EuFe_2As_2 was observed by the analysis of the staggered shifts of diffraction peak of (110) and (103).

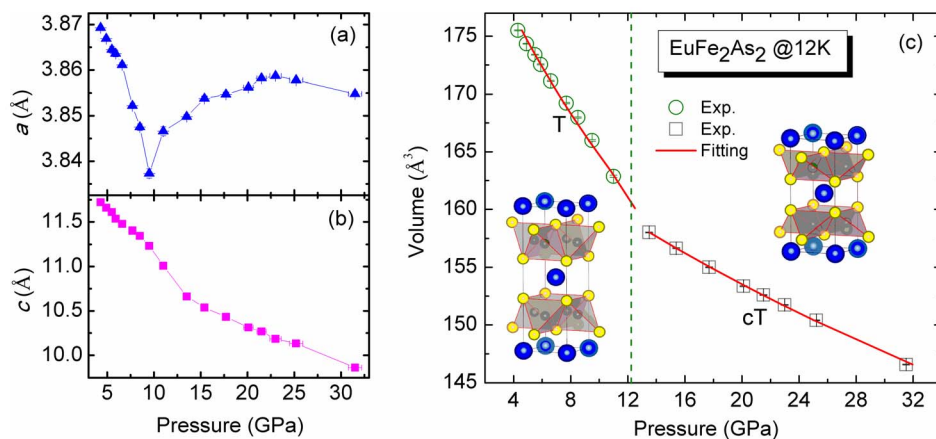


Figure 2 | The pressure dependence of the lattice parameters a (a), which is closely related to the shift of diffraction peak of (110), and c (b) for T and cT phase in EuFe_2As_2 at 12 K. (c) The pressure dependence of volume for EuFe_2As_2 at 12 K and the schematic crystal structures of T and cT phase for EuFe_2As_2 .

XRD experiment during the pressure-increasing cycle, so we can only present a rough value for the phase transition pressure.

Discussion

EuFe_2As_2 exhibits a quasi-two-dimensional structure characteristic under ambient conditions. Like the CuO_2 plane in copper oxide high-temperature superconductors, the Fe_2As_2 layers are conduction planes for the charge carriers. The other building blocks are the charge reservoir layers that dominate the carrier density or chemical potential. In the Fe_2As_2 layer, the Fe and As ions could constitute a FeAs_4 tetrahedron because of the smaller ionic radius of Fe versus As. The iron ions form a planar tetragonal lattice that is sandwiched by As ions to form a FeAs_4 tetrahedron. The tetrahedra are edge-linked closely along the c axis. In general the FeAs_4 tetrahedron is not an ideal normal tetrahedron because of the mismatch between the Fe_2As_2 and carrier layers. The atomic positions of Eu and Fe are constrained by symmetry (the Wyckoff positions 2a and 4d, respectively), whereas the As atom is located at the 4e position. Hence, the applied pressure could affect its z atomic position. The pressure dependence of the bond length of Fe-As ($d_{\text{Fe-As}}$), the bond angle of As-Fe-As ($\angle \text{As-Fe-As}$) and the polyhedral volume of FeAs_4 (V_{FeAs_4}) in EuFe_2As_2 (determined by the Rietveld refinement) are shown in Figure S2. It can be seen from Figure S2 (a) that the bond length of Fe-As first decreases before 7.7 GPa and then increases from 7.7 to 11.0 GPa. However, the bond length of Fe-As becomes less sensitive to applied pressure above 11.0 GPa. The pressure dependence of volume for FeAs_4 presents a similar behavior with increasing pressure as shown in Figure S2 (c). The variation in $\angle \text{As-Fe-As}$ with increasing pressure is shown in Figure S2 (b). From the point of view of crystallography, the FeAs_4 tetrahedron in EuFe_2As_2 is similar to an ideal regular tetrahedron because the As-Fe-As angle ($109.1^\circ (\times 4)$, $110.1^\circ (\times 2)$) is close to 109.47° under ambient conditions. The polyhedron of FeAs_4 becomes much more distorted at increasing pressures (< 7.7 GPa) because the tetrahedral angles ($\angle \text{As-Fe-As}$) deviate from an ideal tetrahedron value of 109.47° with increasing pressure. However, the tetrahedron of FeAs_4 becomes less sensitive and is hardly distorted above 11.0 GPa. Our data are consistent that reported for the T_c as a function of pressure²⁵. This pressure effect on the 122-type EuFe_2As_2 is similar to that of other 122-type AFe_2As_2 ($A = \text{Ba}, \text{Sr}$)^{31,32}, 1111-type LaFeAsO ³³ and 111-type $\text{Na}_{1-x}\text{FeAs}$ ³⁴ systems.

Figure 3 presents the temperature and pressure phase diagram of EuFe_2As_2 . These data include our measurements up to 31.5 GPa and down to 12 K as well as literature data^{22,25,28}. From Figure 3 we found that the transition pressure of T \rightarrow cT in EuFe_2As_2 increases as the

temperature decreases. Simultaneous compression and cooling could also increase the transition pressure. A similar phenomenon also appears in other AFe_2As_2 superconductors such as CaFe_2As_2 and BaFe_2As_2 . Under ambient temperature, the pressure-induced T \rightarrow cT phase transitions in CaFe_2As_2 and BaFe_2As_2 occur at 1.7 and 27 GPa, respectively³⁵. The phase transition from the T phase to the cT phase of CaFe_2As_2 and BaFe_2As_2 occur at 2 GPa, 40 K and 29 GPa, 33 K, respectively³⁵.

Several groups have used XRD and/or neutron diffraction to study the temperature-induced structural phase transition in AFe_2As_2 , which is quite similar to the corresponding structural transformation observed in the undoped “1111” type RFeAsO superconductors. The transition temperatures of T \rightarrow O in CaFe_2As_2 , SrFe_2As_2 , BaFe_2As_2 and EuFe_2As_2 are around 170 K^{13,36,37}, 205 K^{38–42}, 140 K^{43–46} and 190 K^{22,47}, respectively. The structural phase transition of T \rightarrow O is discontinuous and often hysteretic. The ambient condition is tetragonal and coexists with low temperature orthorhombic phases close to the structural phase transition point. These are all hallmarks of a first-order phase transition. The phase transition temperature of

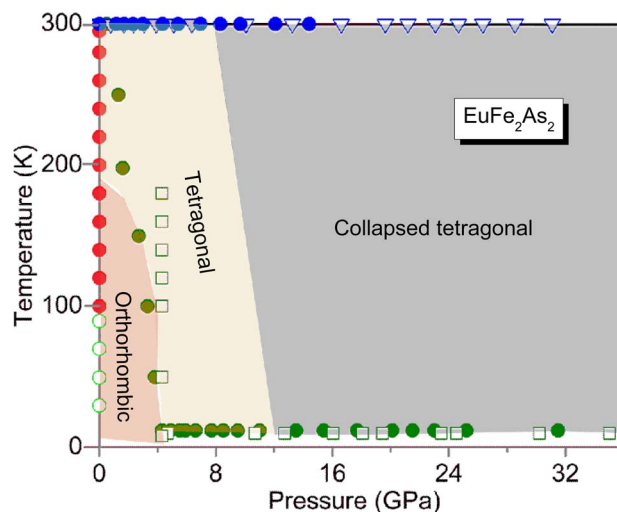


Figure 3 | The crystal structure phase diagram of EuFe_2As_2 derived from the XRD results. The boundary line between T and cT phases shifted to higher pressure as the temperature decreasing. The data marked with solid spheres, open spheres, open triangles and open squares, were taken from the present work, Ref. 22, Ref. 25 and Ref. 28, respectively.



T → O in AFe_2As_2 and the experimental characterization are presented in Table S1.

The phase transition temperature of T → O in SrFe_2As_2 is higher than that of the other three AFe_2As_2 compounds (CaFe_2As_2 , EuFe_2As_2 and BaFe_2As_2). For superconducting or magnetic materials, if the cation is Ca, Sr or Ba, the sample containing Sr shows the highest superconducting transition temperature or Curie temperature. In contrast, a Ca- or Ba-containing sample has a lower corresponding value. The phase transition temperature (T → O) in AFe_2As_2 also shows similar behavior. Previous studies have shown that the lattice parameter a of AFe_2As_2 is very similar ($3.879 \text{ \AA} - 3.9625 \text{ \AA}$), but the lattice parameter c has much more variability ($11.740 \text{ \AA} - 13.0168 \text{ \AA}$)^{22,39,48}. The lattice parameter c of BaFe_2As_2 is much longer than those of the other three isostructural compounds and may cause BaFe_2As_2 to be different from the other three AFe_2As_2 (A = Ca, Eu and Sr) compounds.

The phase transition pressures of T → cT in CaFe_2As_2 , SrFe_2As_2 , BaFe_2As_2 and EuFe_2As_2 are summarized in Figure 4^{25,38,49,50}. When comparing the phase transition pressures of T → cT for these four compounds, we found that the increase in the size of the alkaline earth metal or rare earth cations leads to an increase in the transition pressure. However, it is well known that isostructural compounds containing different cations will undergo similar phase transitions at progressively lower pressures as the cation radii increase. Thus, the pressure-induced transformation from fluorite-type to PbCl_2 -type in CaF_2 , SrF_2 and BaF_2 is 9.5 GPa⁵, 5.0 GPa⁶ and 3.0 GPa⁷, respectively. Similar phenomena have also been found in pressure-induced structural phase transition of CaO , SrO and BaO ^{1–4} (Figure 4, inset). Therefore, the cation radii as a function of phase transition pressure in ThCr_2Si_2 -type iron-based superconductors did not follow the conventional empirical law. In most of cases, pressure-induced structural phase transitions involve the variation of the space group and a combination of the Wyckoff position. We emphasize that in this pressure-induced structural phase transition, the AFe_2As_2 undergoes

an isostructural phase transition without ionic variation of the space group and Wyckoff position. Pressure-induced isostructural phase transitions usually originate from electronic structural changes in the materials⁵¹. The “chemical inner stress” largely due to the increase in cation radii plays a major role in conventional empirical law. However, iron-based superconductors such as AFe_2As_2 are strongly correlated electronic systems, in which the electrons cannot be described effectively in terms of non-interacting entities. The “chemical inner stress” and electronic interactions seen here are coupled, and interplay in pressure-induced structural phase transition in the AFe_2As_2 system. In determining the pressure of phase transitions in AFe_2As_2 , the electronic interactions show a dominant effect versus regular “chemical inner stress” effect. This causes the pressure-induced structural phase transition in AFe_2As_2 compounds exhibit anomalous pattern.

From Figure 4, we found that the transition pressure in EuFe_2As_2 and SrFe_2As_2 is very close. It is well known that the volume of Eu^{2+} with a $4f^6$ electron shell is larger than that of Eu^{3+} with a $4f^6$ electron shell. Thus, the application of pressure could drive a valence transition of the Eu ions in EuFe_2As_2 from divalent to trivalent. The Eu ions mean valence changes from 2.1 to 2.27 when the pressure increases from 2.1 to 9.8 GPa²⁵. The ionic radius of Sr^{2+} and Eu with mixed valence is very close. Therefore, the structural behavior of EuFe_2As_2 is very similar to that of SrFe_2As_2 .

In summary, the transition pressure of T → cT in EuFe_2As_2 increases as the temperature decreases. We identified the phase lines corresponding to the phase transitions for the tetragonal, orthorhombic and collapsed tetragonal phases of EuFe_2As_2 . We discuss the variation in geometry configuration as a function of pressure for the Fe_2As_2 layers in EuFe_2As_2 . The transition pressures (T → cT) in AFe_2As_2 show a correlation with the size of the ionic radius under ambient conditions. The cationic radii as a function of phase transition pressure in a ThCr_2Si_2 -type iron-based superconductor did not follow the conventional compression law.

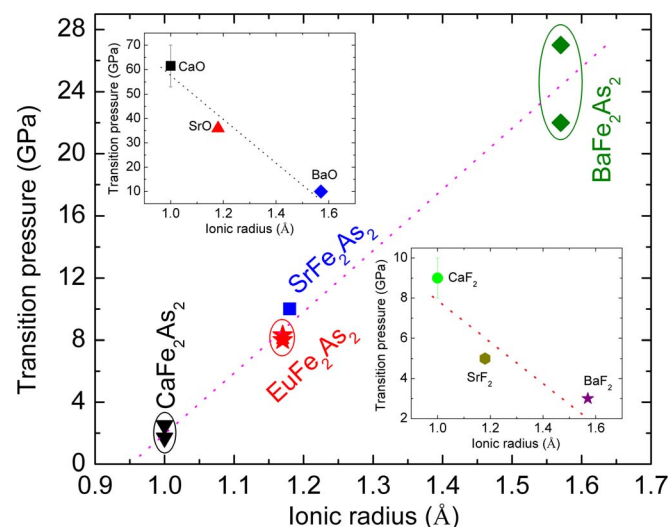


Figure 4 | The correlation between the ionic radius for AFe_2As_2 (A = Ca, Sr, Eu and Ba) iron arsenide superconductors and their corresponding transition pressure of T → cT phases (at ambient temperature). The transition pressures (T → cT) in AFe_2As_2 show a correlation with the size of the ionic radius under ambient conditions, in which compounds exhibited higher transition pressure with larger cation ionic radius. The pressure-induced structural phase transitions for AFe_2As_2 were taken from reference 22, 25 and 28 along with this work. The dotted lines are meant to guide the eyes. The inset shows the ionic radius as a function of phase transition pressure for $\text{A}_{\text{EM}}\text{O}$ and $\text{A}_{\text{EM}}\text{F}_2$ (A_{EM} = Ca, Sr and Ba). The data refer to reference 1–7.

Methods

High resolution synchrotron powder XRD patterns at low temperature and ambient pressure were collected at the beamline 11-BM-B at the Advanced Photon Source (APS) at Argonne National Laboratory (ANL). The experiments were conducted with a monochromatic beam of 0.4124 Å. High pressure and low temperature angle-dispersive XRD (AD-XRD) patterns were collected at the High Pressure Collaborative Access Team (HPCAT) beamline 16-ID-B at APS of ANL using a MAR345 flat panel detector. The experiments were conducted with a monochromatic beam of 0.3697 Å. All the XRD results were confirmed with experiments performed at BL15U1 beamline at Shanghai Synchrotron Radiation Facility (SSRF) using a monochromatic beam of 0.6199 Å. A symmetric type diamond anvil cell (DAC) with a diamond culet size of 300 μm was used to apply the pressure. T301 stainless steel with a thickness of 300 μm and a pre-indentation thickness of 45 μm served as the gasket. The 120 μm diameter sample chamber was filled with a mixture of the EuFe_2As_2 compound, a ruby chip and silicone oil as the pressure transmitting medium. For high pressure and low temperature experiments, the DAC was cooled in a continuous He flow type cryostat. The pressure was measured with the *in situ* ruby fluorescence technique⁵². The diffraction patterns were integrated with the FIT2D computer code⁵³. The XRD data was refined with the Rietveld method employed by the General Structure Analysis System (GSAS)⁵⁴ based on the structural model used in prior reports²².

- Jeanloz, R., Ahrens, T. J., Mao, H. K. & Bell, P. M. B1-B2 transition in calcium oxide from shock-wave and diamond-cell experiments. *Science* **206**, 829–830 (1979).
- Mammone, J. F., Mao, H. K. & Bell, P. M. Equations of state of CaO under static pressure conditions. *Geophys. Res. Lett.* **8**, 140–142 (1981).
- Sato, Y. & Jeanloz, R. Phase transition in SrO . *J. Geophys. Res.* **86**, 11773–11778 (1981).
- Weir, S. T., Vohra, Y. K. & Ruoff, A. L. High-pressure phase transitions and the equations of state of BaS and BaO . *Phys. Rev. B* **33**, 4221–4226 (1986).
- Gerward, L., Olsen, J. S., Steenstrup, S., Åsbrink, S. & Waskowska, A. X-ray diffraction investigations of CaF_2 at high pressure. *J. Appl. Crystallogr.* **25**, 578–581 (1992).
- Kourouklis, G. A. & Anastassakis, F. Pressure-induced phase transition in SrF_2 : A Raman study. *Phys. Rev. B* **34**, 1233–1237 (1986).



7. Léger, J. M., Haines, J., Atouf, A., Schulte, O. & Hull, S. High-pressure x-ray- and neutron-diffraction studies of BaF₂: An example of a coordination number of 11 in AX₂ compounds. *Phys. Rev. B* **52**, 13247–13256 (1995).
8. Kamihara, Y., Watanabe, T., Hirano, M. & Hosono, H. Iron-Based Layered Superconductor La[O_{1-x}F_x]FeAs (x = 0.05–0.12) with T_c = 26 K. *J. Am. Chem. Soc.* **130**, 3296–3297 (2008).
9. Takahashi, H. *et al.* Superconductivity at 43 K in an iron-based layered compound LaO_{1-x}F_xFeAs. *Nature* **453**, 376–378 (2008).
10. Chen, X. H. *et al.* Superconductivity at 43 K in SmFeAsO_{1-x}F_x. *Nature* **453**, 761–762 (2008).
11. Zhao, J. G. *et al.* Structure Stability and Compressibility of Iron-Based Superconductor Nd(O_{0.88}F_{0.12})FeAs under High Pressure. *J. Am. Chem. Soc.* **130**, 13828–13829 (2008).
12. Chen, G. F. *et al.* Superconductivity at 41 K and Its Competition with Spin-Density-Wave Instability in Layered CeO_{1-x}F_xFeAs. *Phys. Rev. Lett.* **100**, 247002 (2008).
13. Torikachvili, M. S., Bud'ko, S. L., Ni, N. & Canfield, P. C. Pressure Induced Superconductivity in CaFe₂As₂. *Phys. Rev. Lett.* **101**, 057006 (2008).
14. Hiramatsu, H., Katase, T., Kamiya, T., Hirano, M. & Hosono, H. Water-induced superconductivity in SrFe₂As₂. *Phys. Rev. B* **80**, 052501 (2009).
15. Rotter, M., Tegel, M. & Johrendt, D. Superconductivity at 38 K in the Iron Arsenide (Ba_{1-x}K_x)Fe₂As₂. *Phys. Rev. Lett.* **101**, 107006 (2008).
16. Wu, G. *et al.* Different resistivity response to spin-density wave and superconductivity at 20 K in Ca_{1-x}Na_xFe₂As₂. *J. Phys.: Condens. Matter* **20**, 422201 (2008).
17. Hoffmann, R. & Zheng, C. Making and breaking bonds in the solid state: the thorium chromium silicide (ThCr₂Si₂) structure. *J. Phys. Chem.* **89**, 4175–4181 (1985).
18. Marchand, R. & Jeitschko, W. Ternary lanthanoid-transition metal pnictides with ThCr₂Si₂-type structure. *J. Solid State Chem.* **24**, 351–357 (1978).
19. Wu, D. *et al.* Effects of magnetic ordering on dynamical conductivity: Optical investigations of EuFe₂As₂ single crystals. *Phys. Rev. B* **79**, 155103 (2009).
20. Xiao, Y. *et al.* Magnetic structure of EuFe₂As₂ determined by single-crystal neutron diffraction. *Phys. Rev. B* **80**, 174424 (2009).
21. Ren, Z. *et al.* Antiferromagnetic transition in EuFe₂As₂: A possible parent compound for superconductors. *Phys. Rev. B* **78**, 052501 (2008).
22. Tegel, M. *et al.* Structural and magnetic phase transitions in the ternary iron arsenides SrFe₂As₂ and EuFe₂As₂. *J. Phys.: Condens. Matter* **20**, 452201 (2008).
23. Sun, L. L. *et al.* Re-emerging superconductivity at 48 kelvin in iron chalcogenides. *Nat. Lett.* **483**, 67–69 (2012).
24. Alireza, P. L. *et al.* Superconductivity up to 29 K in SrFe₂As₂ and BaFe₂As₂ at high pressures. *J. Phys.: Condens. Matter* **21**, 012208 (2009).
25. Uhoja, W. *et al.* Anomalous compressibility effects and superconductivity of EuFe₂As₂ under high pressures. *J. Phys.: Condens. Matter* **22**, 292202 (2010).
26. Sun, L. L. *et al.* Valence change of europium in EuFe₂As_{1.4}P_{0.6} and compressed EuFe₂As₂ and its relation to superconductivity. *Phys. Rev. B* **82**, 134509 (2010).
27. Matsubayashi, K. *et al.* Pressure-induced changes in the magnetic and valence state of EuFe₂As₂. *Phys. Rev. B* **84**, 024502 (2011).
28. Uhoja, W. O., Tsoi, G. M., Vohra, Y. K., McGuire, M. A. & Sefat, A. S. Structural phase transitions in EuFe₂As₂ superconductor at low temperatures and high pressures. *J. Phys.: Condens. Matter* **23**, 365703 (2011).
29. Huhnt, C., Schlabit, W., Wurth, A., Mewis, A. & Reehuis, M. First- and second-order phase transitions in ternary europium phosphides with ThCr₂Si₂-type structure. *Physica B* **252**, 44–54 (1998).
30. Birch, F. Finite Elastic Strain of Cubic Crystals. *Phys. Rev.* **71**, 809–824 (1947).
31. Mani, A., Ghosh, N., Paulraj, S., Bharathi, A. & Sundar, C. S. Evolution of the Kondo resonance feature and its relationship to spin-orbit coupling across the quantum critical point in Ce₂Rh_{1-x}Co_xSi₃. *Europhys. Lett.* **87**, 17004 (2009).
32. Igawa, K. *et al.* Pressure-Induced Superconductivity in Iron Pnictide Compound SrFe₂As₂. *J. Phys. Soc. Jpn.* **78**, 025001 (2009).
33. Okada, H. *et al.* Superconductivity under High Pressure in LaFeAsO. *J. Phys. Soc. Jpn.* **77**, 113712 (2008).
34. Liu, Q. Q. *et al.* Pressure-Induced Isostructural Phase Transition and Correlation of FeAs Coordination with the Superconducting Properties of 111-Type Na_{1-x}FeAs. *J. Am. Chem. Soc.* **133**, 7892–7896 (2011).
35. Mittal, R. *et al.* Ambient- and low-temperature synchrotron x-ray diffraction study of BaFe₂As₂ and CaFe₂As₂ at high pressures up to 56 GPa. *Phys. Rev. B* **83**, 054503 (2011).
36. Goldman, A. I. *et al.* Lattice and magnetic instabilities in CaFe₂As₂: A single-crystal neutron diffraction study. *Phys. Rev. B* **78**, 100506 (2008).
37. Ni, N. *et al.* First-order structural phase transition in CaFe₂As₂. *Phys. Rev. B* **78**, 014523 (2008).
38. Krellner, C. *et al.* Magnetic and structural transitions in layered iron arsenide systems: AFe₂As₂ versus RFeAsO. *Phys. Rev. B* **78**, 100504 (2008).
39. Kumar, M. *et al.* Effect of pressure on the magnetostructural transition in SrFe₂As₂. *Phys. Rev. B* **78**, 184516 (2008).
40. Jesche, A. *et al.* Strong coupling between magnetic and structural order parameters in SrFe₂As₂. *Phys. Rev. B* **78**, 180504 (2008).
41. Zhao, J. *et al.* Spin and lattice structures of single-crystalline SrFe₂As₂. *Phys. Rev. B* **78**, 140504 (2008).
42. Yan, J. Q. *et al.* Structural transition and anisotropic properties of single-crystalline SrFe₂As₂. *Phys. Rev. B* **78**, 024516 (2008).
43. Kim, S. K. *et al.* Combined effects of pressure and Ru substitution on BaFe₂As₂. *Phys. Rev. B* **84**, 134525 (2011).
44. Huang, Q. *et al.* Neutron-Diffraction Measurements of Magnetic Order and a Structural Transition in the Parent BaFe₂As₂ Compound of FeAs-Based High-Temperature Superconductors. *Phys. Rev. Lett.* **101**, 257003 (2008).
45. Wilson, S. D. *et al.* Neutron diffraction study of the magnetic and structural phase transitions in BaFe₂As₂. *Phys. Rev. B* **79**, 184519 (2009).
46. Rotter, M. *et al.* Spin-density-wave anomaly at 140 K in the ternary iron arsenide BaFe₂As₂. *Phys. Rev. B* **78**, 020503 (2008).
47. Xiao, Y. *et al.* Anomalous in-plane magnetoresistance in a EuFe₂As₂ single crystal: Evidence of strong spin-charge-lattice coupling. *Phys. Rev. B* **85**, 094504 (2012).
48. Mittal, R. *et al.* Pressure dependence of phonon modes across the tetragonal to collapsed-tetragonal phase transition in CaFe₂As₂. *Phys. Rev. B* **81**, 144502 (2010).
49. Kasinathan, D. *et al.* Symmetry-preserving lattice collapse in tetragonal SrFe_{2-x}Ru_xAs₂ (x=0, 0.2): A combined experimental and theoretical study. *Phys. Rev. B* **84**, 054509 (2011).
50. Uhoja, W. *et al.* Collapsed tetragonal phase and superconductivity of BaFe₂As₂ under high pressure. *Phys. Rev. B* **82**, 144118 (2010).
51. Hall, H. T., Merrill, L. & Barnett, J. D. High pressure polymorphism in Cesium. *Science* **146**, 1297–1299 (1964).
52. Mao, H. K., Xu, J. A. & Bell, P. Calibration of the ruby pressure gauge to 800-kbar under quasi-hydrostatic conditions. *J. Geophys. Res.* **91**, 4673–4676 (1986).
53. Hammersley, A. P., Svensson, S. O., Hanfland, M., Fitch, A. N. & Hausermann, D. Two-dimensional detector software: From real detector to idealised image or two-theta scan. *High Pressure Res.* **14**, 235–248 (1996).
54. Larson, A. C. & Von Dreele, R. B. *General Structure Analysis System* (GSAS), Los Alamos National Laboratory Report LAUR, 86–748 (1994).

Acknowledgments

We thank Matthew Suchomel (11-BM-B, APS, ANL) for experimental help. The HPCAT facility is supported by CIW, CDAC, UNLV and LLNL through funding from DOE-NNSA, DOE-BES and NSF. APS is supported by DOE-BES, under Contract No. DE-AC02-06CH11357. Portions of this work were performed at the BL15U1 beamline at SSRF. This work was partially supported by Natural Science Foundation of China (11004072, 11374075, 10975042, 10904022), Program for New Century Excellent Talents in University (NCET-10-0444), Heilongjiang Province Science Fund for Distinguished Young Scholars (JC201005), Heilongjiang Natural Science Foundation (E200948), Longjiang Scholar, the Fundamental Research Funds for the Central Universities (HIT.BRET1.2010002, HIT.IBRSEM.A.201403) and HIT-Argonne Overseas Collaborative Base Project. This work was also supported as part of eFree, an Energy Frontier Research Center funded by the U.S. Department of Energy (DOE), Office of Science under DE-SC0001057.

Author contributions

L.W. designed the project; Z.H.Y., L.W., L.H.W., H.Z.L., K.Y., Y.S.Z. and H.K.M. were involved in performing experiments, data analysis and the drafting of the manuscript. C.Y.L. and J.G.Z. conducted DAC experiments. W.W., J.L.L. and N.L.W. synthesized the sample. S.S. was responsible for the beamline of 16 IDB at Advanced Photon Source. All authors reviewed the manuscript.

Additional information

Supplementary information accompanies this paper at <http://www.nature.com/scientificreports>

Competing financial interests: The authors declare no competing financial interests.

How to cite this article: Yu, Z. *et al.* Conventional empirical law reverses in the phase transitions of 122-type iron-based superconductors. *Sci. Rep.* **4**, 7172; DOI:10.1038/srep07172 (2014).



This work is licensed under a Creative Commons Attribution-NonCommercial-NoDerivs 4.0 International License. The images or other third party material in this article are included in the article's Creative Commons license, unless indicated otherwise in the credit line; if the material is not included under the Creative Commons license, users will need to obtain permission from the license holder in order to reproduce the material. To view a copy of this license, visit <http://creativecommons.org/licenses/by-nc-nd/4.0/>